Development of a Respirable Dust Mitigation System for a High Longwall Face at Sihe Colliery in China – a Case Study

Junfeng Wang[1], Yibo Tang[1,*], Hailong Du[2] & Weiwei Shang[2]

[1]College of Mining Engineering, Taiyuan University of Technology, Taiyuan, China, 030024
[2]Shanxi Jincheng Anthracite Mining Group Ltd, Jincheng, China, 048006
*E-mail: tangyibo11@126.com

Abstract. Dust is a major hazard in underground coal mines that threatens the work health and safety of coal miners. The dust issue becomes increasingly significant with the development of highly mechanized coal mining. This issue is particularly serious at the high longwall faces of the Sihe colliery in China as the concentration of dust, in particular respirable dust, at these faces far exceeds the regulatory dust limits. Field testing and computational fluid dynamics (CFD) simulations were conducted to understand the sources of dust generation and its dynamic movement in the #5301 longwall face of high-cutting height at the colliery. The investigation results showed that shearer generated dust was minimal during the coal cutting operation; that face spalling and chock movement were the main dust generating sources, causing significant contamination to the walkway; and that the majority of dust particles from the face (regardless of source) eventually disperse into the main gate, where the dust concentration was greater than 500 mg/m^3. These findings were used to develop an effective coal dust mitigation system involving the installation of dust scrubbers, curtains, and venture and crescent sprays. The results of CFD modeling indicate that the dust concentration could be significantly reduced by adopting the new dust mitigation system.

Keywords: *CFD modeling; dust mitigation; health and safety; longwall mining; respirable dust.*

1 Introduction

Coal dust is commonly generated in a series of underground coal mining activities such as coal cutting, coal transportation, chock movement, etc., and more dust is being generated with the development of fully mechanized and highly productive longwall faces. It is well documented that increased dust concentrations in coal mines can cause both industrial and health problems, such as dust explosions and pneumoconiosis [1-2]. In China, there were 4648 casualties caused by 105 coal dust explosion accidents (including methane-linked and non methane-linked explosions) between the years 1970 and 2014

Received March 14th, 2017, Revised July 10th, 2017, Accepted for publication September 4th, 2017.
 ISSN: 2337-5779, DOI: 10.5614/j.eng.technol.sci.2017.49.4.2

and more than 105 thousand coal miners were diagnosed with pneumoconiosis from the year 2009 to 2013 [3-4]. To mitigate these risks, maximum allowable limits have been set for dust concentrations in working places in underground coal mines by various governments. In China, the *Safety Regulations in Coal Mines* stipulate that the maximum allowable total dust concentration is between 2 to 20 mg/m^3 and the respirable dust concentration is in the range of 1 to 6 mg/m^3 depending on the silica content in the dust [5]. In New South Wales, Australia, for underground mines, the specified limit for quartz-containing dust is 0.12 mg/m^3 for respirable quart and the specified limit for respirable dust, other than quartz-containing dust, is 2.5 mg/m^3, while the specified limit concentration for inhalable dust is 10 mg/m^3[6].

A number of dust control measures are used in underground coal mines. These can be categorized into five methods: prevention, removal, isolation, dilution, and suppression [7-8]. Water infusion has been used in coal mines to reduce dust generation during the coal cutting process, though its effectiveness on dust mitigation is highly dependent on the permeability, wettability and in-situ moisture content of the coal seam [9]. Various dust collectors or extractors or scrubbers have been developed to remove dust particles from the working environment in coal mines. Due to its low maintenance requirement and high respirable dust capture efficiency (greater than 90%), the dust scrubber has gained popularity in mining applications for effective dust control [10].

The water spray is by far the most widely used medium for dust suppression in underground coal mines. Depending on the specific application, several types of water sprays are available for use at longwall faces, coal crushing and transfer points. For example, hollow-cone sprays are mostly located close to dust source for suppression, while full-cone sprays are more used further away from the dust source or can be used for wetting of coal at transfer points. Although air-atomizing sprays are reported to be the most effective in airborne dust capture, their utilization is limited due to high maintenance requirements [7]. More recently, Wang, *et al*. [11-12] have stated that foam technology is more efficient than water spraying for dust control in coal mines because it distributes moisture much more evenly over a large contact area on dust particles, improving the wetting and adhesion ability.

Despite the dust control measures available, field practice has demonstrated that the control of respirable dust in longwall faces is very difficult and often ineffective [13-14]. This is particularly true in the Shihe colliery, where the dust concentration, particularly respirable dust, at its high longwall faces often exceeds the maximum allowable dust limit. To address the dust issue, field testing and CFD modeling were conducted at the #5301 longwall face of the

colliery to identify the sources of dust generation, understand dust dynamic movement, and develop an effective dust mitigation system.

2 Field Investigations

The #5301 longwall face of Sihe colliery is 296 m wide (not including the width of the main gate/tail gate at the face's end) and the cutting height of the face is 6 m. The field investigation aimed to quantify respirable and inhalable dust loads at each independent source of dust generation at the face, and airflow rates at the intake and return roadways and several cross sections of the face.

2.1 Dust Monitoring

Dust load tests at the face were conducted three times in this study. Coal production for each test was 1619.86, 2014.95 and 1527.68 tons respectively. As displayed in Figure 1, five sets of dust samplers (pumps and monitors) labeled 1 to 5 were placed in the following positions: (1) at the last open cut through in the tail gate, (2) at the intake road in the tail gate, (3) at shield #173, or near the face end of the tail gate, (4) at the middle of the face, and (5) at shield #4, or near the face end of the main gate.

A total of 15 samples were taken over three separate tests. The dust testing equipment was obtained from Envirocon company, Australia (Figure 1). Table 1 shows the raw input data collected during the sampling period together with the calculated dust generation rates, which form the benchmark respirable dust production during the cutting cycle. It shows the test number, the positions of the dust samplers, the weight of the respirable size dust particles, the coal production during the testing period, and dust load.

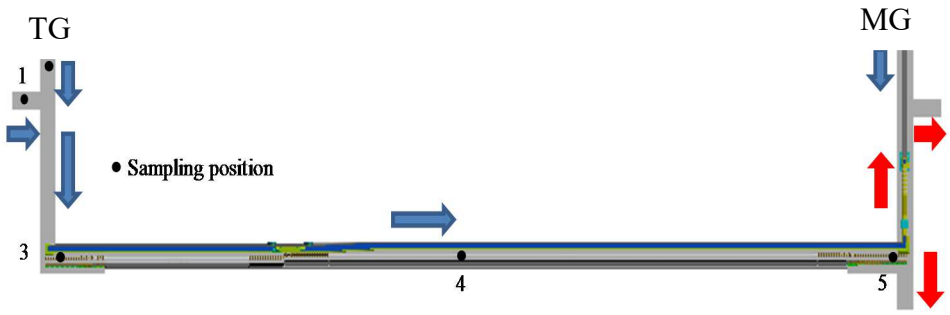

(Full arrow lines represent intake air flow, half arrow lines represent return air flow, TG is tail gate, MG is main gate)

Figure 1 Placement of dust samplers at the #5301 longwall face.

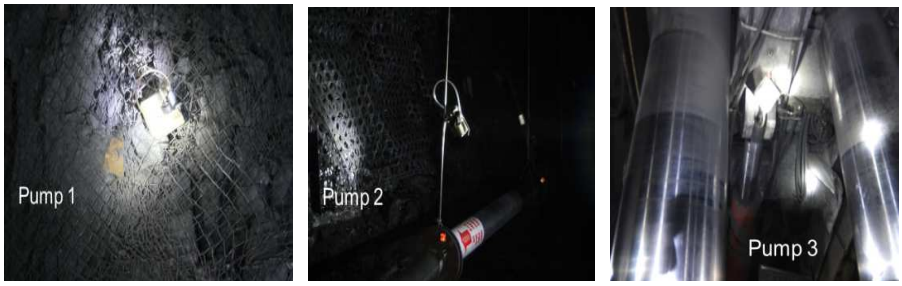

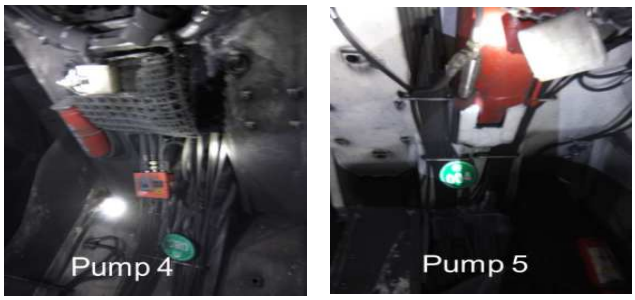

Figure 1 ***Continued.*** Placement of dust samplers at the #5301 longwall face.

Table 1 Dust testing results at the #5301 longwall face.

Test No.	Position	Respirable dust, mg	Coal cut, tons	Dust load, mg/ton
1	Last cut-through tail gate	0.87	1619.86	0.000537
1	Intake roadway, tail gate	0.96	1619.86	0.000593
1	Shield #173	1.23	1619.86	0.000759
1	Shield #85	7.04	1619.86	0.004346
1	Shield #4	8.32	1619.86	0.005136
2	Last cut-through tail gate	0.30	2014.95	0.000149
2	Intake roadway, tail gate	0.58	2014.95	0.000288
2	Shield #173	0.71	2014.95	0.000352
2	Shield #85	5.93	2014.95	0.002943
2	Shield #4	8.98	2014.95	0.004457
3	Last cut-through tail gate	0.89	1527.68	0.000583
3	Intake roadway, tail gate	0.54	1527.68	0.000353
3	Shield #173	0.66	1527.68	0.000432
3	Shield #85	3.79	1527.68	0.002481
3	Shield #4	8.52	1527.68	0.005577

Table 2 summarizes the dust load at each of the sampling points for each test. It can be seen that there was a difference in the dust production at each individual

point of dust generation at the longwall face and the intake ventilation. The face dust differential can be explained by the unpredictability of the face slabbing occurring during the cutting cycle.

Table 2 Comparison of dust loads at each of the sampling points for each test.

Test No.	Last cut-through tail gate	Intake roadway tail gate	Shield #173	Shield #85	Shield #4
1	0.000537	0.000593	0.000759	0.004346	0.005136
2	0.000149	0.000288	0.000352	0.002943	0.004457
3	0.000583	0.000353	0.000432	0.002481	0.005577

Field observations made during the cutting cycle indicated that very little dust was produced from the shearer actually cutting in either direction. The majority of the dust produced during the cutting cycle can be attributed to slabbing due entirely to the height of the face. As shields were retracted, the face slumped and slabbed onto the armored face conveyor (AFC) and pan line, creating a significant amount of dust that was forced into the intake ventilation and swept down the face.

2.2 Airflow Monitoring

Understanding the airflow patterns and dust flow behavior at the longwall face are essential for the development of an effective dust mitigation system. In this study, a ventilation survey was conducted to obtain these necessary data. Measurements of air flow rates were carried out at the tail gate and the main gate of the longwall face; the results are shown in Figure 2.

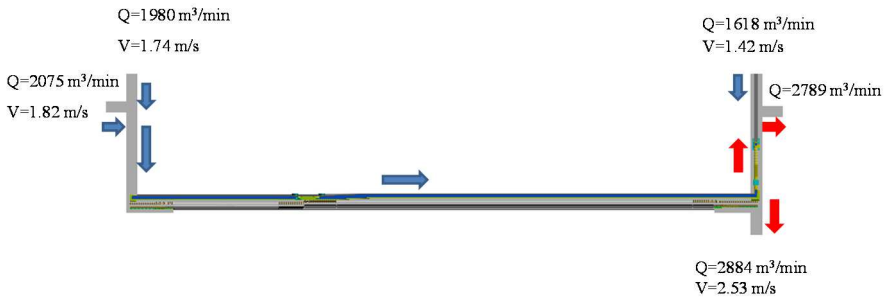

Figure 2 Layout of #5301 longwall face and ventilation system.

In addition to the above measurements, airflow velocity (m/s) in several face cross sections (50 m, 150 m, 200 m and 250 m away from the main gate) was also measured using a kestrel hand-held anemometer; the measured results are shown in Figure 3. These measured data were later used for setting up the boundary conditions of a CFD model for the face and validation of the model.

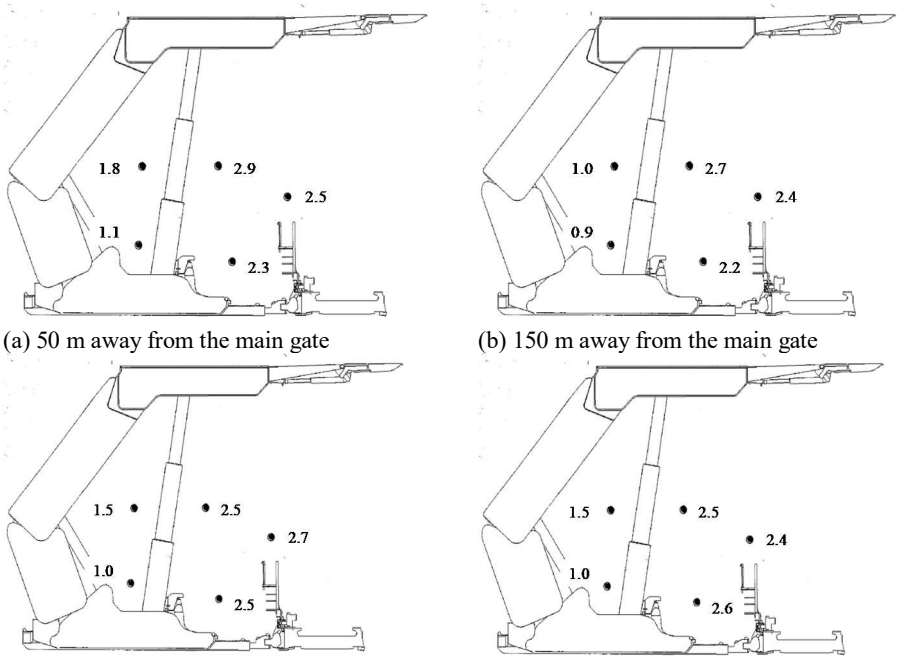

(a) 50 m away from the main gate (b) 150 m away from the main gate

(c) 200 m away from the main gate (d) 250 m away from the main gate

Figure 3 Measured air flow velocities at selected cross sections along the longwall face.

3 CFD Modeling

3.1 Model Fundamentals

The motion of fluid in a longwall face follows the principles of mass conservation, Newton's second law, and the first law of thermodynamics. The differential forms of these three governing laws are known as the continuity equation, the Navier-Stokes equation, and the energy equation, respectively, as shown in Eqs. (1) to (3) below:

$$\frac{\sigma\rho}{\sigma t} + \nabla \cdot (\rho V) = 0 \tag{1}$$

$$\rho\left(\frac{\partial V}{\partial t} + V \cdot \nabla V\right) = -\nabla p + \mu\nabla^2 V + F \tag{2}$$

$$\rho\left(\frac{\partial E}{\partial t} + E \cdot \nabla E\right) = K\nabla^2 T + W_s + S_E \tag{3}$$

where ρ is fluid density, $V=(v_x,v_y,v_z)$ is the velocity vector of flow particles, ∇p is the pressure gradient, μ is fluid viscosity, $F=(F_x,F_y,F_z)$ is the body force vector, E is flow media energy, K is the conductivity coefficient, W_s is the work done by the surface stresses, and S_E represents energy supplied by the source term.

In this study, the finite volume method was used to discretize the flow domain into control volumes or grids through which the numerical difference equations representing the governing equations could be solved at these discrete volumes across the flow domain by the use of iterative numerical algorithms.

Air flow at a longwall face is turbulent flow due to its high Reynolds number. The two two-equation k-ε model proposed by Launder and Spalding [15] has been demonstrated to be suitable to investigate the ventilation system [16-19] and was therefore employed in this study to determine the turbulent flow field.

Corresponding to the calculated flow field, the dispersion of respirable dust particles can be determined by either the Euler-Lagrange method or the Euler-Euler method. The movement of particles is described by tracking a large number of particles through the calculated flow field in the Euler-Lagrange method, where the interactions between particles are neglected. When the Euler-Euler method is employed, the discrete dust particles are treated as interpenetrating continua [20]. A comparison of the two methods indicated that the Euler-Lagrange method was more suitable for this study.

With the use of the Euler-Lagrange method, the trajectories of individual particles can be calculated by solving the momentum equation. By integrating the force balance on a particle, the momentum equation can be written in the following form:

$$\frac{d\vec{u}_p}{dt}=F_D(\vec{u}-\vec{u}_p)+\frac{\vec{g}(\rho_p-\rho)}{\rho_p}+\vec{F} \tag{4}$$

In Eq. (4), the left hand side stands for the inertial force per unit particle force, where $\vec{u}_p$ is the particle velocity vector; the first term on the right hand side stands for the drag force per unit particle mass; the second term stands for the gravity and the buoyancy, where ρ and ρ_p are the density of fluid and particles. The last term stands for additional forces, which includes forces such as the virtual mass force, the thermophoretic force caused by the temperature gradient, the pressure gradient force, the Brownian force, and Saffman's lift force.

In this study, the dust particles were assumed to be spherical and the drag force was thus assumed to follow the spherical drag law, which can be expressed in Eq. (5) as follows:

$$F_{drag} = F_D(\vec{u} - \vec{u}_p) = \frac{18\mu}{\rho_p d_p^2}\frac{C_D R_e}{24}(\vec{u} - \vec{u}_p) \tag{5}$$

where C_D is the drag coefficient, which can be calculated by the equation $C_D = a_1 + a_2 / R_e + a_3 / R_e^2$, and a_1, a_2, a_3 are constants; R_e is the relative Reynolds number, which is defined as $R_e = \rho d_p \left|\vec{u}_p - \vec{u}\right| / \mu$.

It is worth noting that the virtual mass force is important when the fluid density is larger than the particle density, which was not the case in this study and the virtual mass force was therefore neglected. Meanwhile, this study was conducted under isothermal conditions, so the thermophoretic force and the Brownian force were not considered either.

Therefore, by substituting the additional force $\vec{F} = \vec{F}_f + \vec{F}_S$ in Eq. (4), the particles can be tracked by solving the following Eq. (6):

$$\frac{d\vec{u}_p}{dt} = \frac{18\mu}{\rho_p d_p^2}\frac{C_D R_e}{24}(\vec{u} - \vec{u}_p) + \frac{\vec{g}(\rho_p - \rho)}{\rho_p} + \vec{F}_f + \vec{F}_S \tag{6}$$

where $\vec{F}_f$ and $\vec{F}_S$ stand for the fluid pressure gradient force and Saffman's lift force, respectively.

3.2 Model Development

Based on data collected during field investigation, a full-scale 3D model, including the shearer, longwall chocks, Beam Stage Loader (BSL) and belt system at the main gate, was developed using Design Modeller within ANSYS 13 Workbench [20]. The geometrical characteristics of the CFD models are shown in Table 3 and a snapshot of the model is shown in Figure 4(a).

It can be seen from Table 3 that the main gate/tail gate in the model was 50 m in length, allowing the full development of the airflow field in the roadway. The model was meshed using a tetrahedron method with 6.5 million elements due to the complex geometry (as shown in Figure 4(b)).

Accurate specifications of boundary conditions are crucial in CFD modeling to accurately predict the physical phenomena. In this study, four kinds of boundary

conditions were involved: velocity inlet, assigned to the three intake ventilation roadways through which fresh air is provided to the face and the boundary of the back return; pressure outlet, assigned to the main gate cut-through, which is the outlet of the model allowing air flow back to the return system; the cutting drums of the shearer, treated as moving walls; the ribs, floor, roof and all the other surfaces of equipment, treated as standard walls.

Table 3 CFD model geometry of the #5301 longwall face.

Name	Dimension, m
Face width	296
Cutting height	6
Tail gate and tail gate ct width	5
Tail gate and tail gate ct	3.8
Main gate width	5.5
Main gate height	3.8
Main gate/tail gate length	50
Goaf length behind chock	1.5

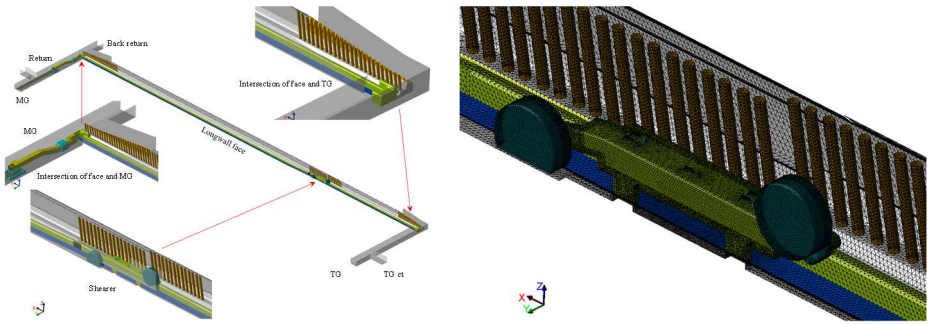

(a) 3 D view of the longwall model

(b) Computation grid in the vicinity of the shearer

Figure 4 Overview of the CFD longwall model.

Data obtained from the field test were used for validation of the base model. A comparison between measured and model-predicted flow velocities on the four cross sections along the face was made and it was found that the model-predicted velocities agreed well with the field-measured data, demonstrating the validity of the model.

3.3 Airflow Patterns

A good understanding of airflow patterns plays an important role in the development of an effective dust mitigation system. Figure 5 shows the velocity contour and vector distribution at 2 m above floor level along the face. It can be seen from Figure 5 that the velocity is not evenly distributed along the face, in particular at the tail gate/main gate and the intersection of the face and the tail gate/main gate. It is noted that significant flow circulation occurred at the intersection of roadways and face, where the flow direction changes.

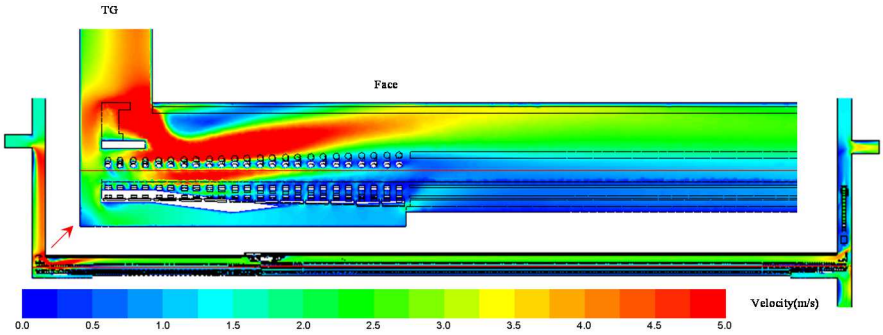

Figure 5 Velocity contour along the face and a closer view at the intersection of the tail gate and the face.

3.4 Respirable Dust Flow and Distribution Patterns

Table 4 shows the respirable dust sources and the corresponding dust generation rate used in the model. It can be seen that along the longwall face, dust was released from the travel road (tail gate), chock movement, face spalling and drum cutting. Dust particles generated at the AFC transfer point and BSL discharge at the main gate were also taken into account in the model. Field observation indicated that at the #5301 face, face spalling/slabbing was the major dust source, causing significant contamination to the face ventilation. Therefore, in the model 50% of longwall dust was released from face spalling. The dispersion of particles in the airflow was tracked using a stochastic tracking (random walk) model, which includes the effect of instantaneous turbulent velocity fluctuations on the particle trajectories through the use of stochastic methods.

Figure 6 illustrates the tracked trajectories of dust particles released from the intake ventilation. It can be observed that the dispersion of respirable dust from the intake ventilation is highly dependent on the airflow patterns and will disperse widely in the entire working environment as the ventilation eventually leaves the face through the two returns if not captured along the face. Therefore,

effective dust mitigation measures should be carried out to minimize dust contamination at the intake ventilation, which is of great importance to reduce the overall dust level along the face.

Table 4 Definition of respirable dust sources used in the model.

Dust source	Dust generation rate, mg/s	Respirable dust sizes, μm	
		Range	Mean
Travel road	2973	1-10	4
Chock movement	4163		
Face spalling ahead of leading drum	5948		
Tail gate drum (leading drum)	3568		
Main gate drum	1189		
Face spalling at face middle	5948		
AFC transfer point	1000		
BSL discharge	1000		
Sum	25789		

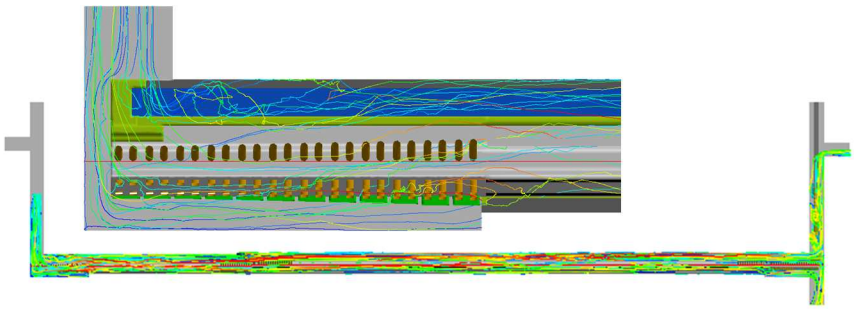

Figure 6 Dispersion characteristics of dust particles from tail gate intake ventilation.

Figure 7 shows the dust concentration distribution at 2.5 m above floor level. It can be seen that the dust concentration was generally less than 100 mg/m^3 upwind of the shearer and increased greatly downwind of the chock movement. The highest dust concentration was distributed in the zones above the AFC and at the main gate, where the dust concentration was greater than 500 mg/m^3. In the vicinity of the shearer and in particular downwind of the chock movement, the dust concentration reached around 200 mg/m^3 in the walkway. The dust concentration was also high at the intersection of the face and the main gate due to the use of the back return system, which allows a certain amount of dust from the face to flow towards the back of the face.

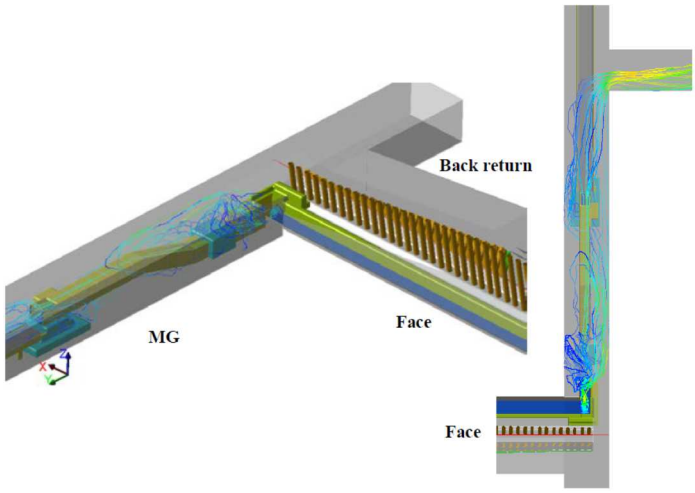

Figure 7 Dispersion characteristics of dust particles from the AFC transfer point.

Figure 8 illustrates the dust concentration distribution along the center of walkway. It can be seen that the overall dust concentration was not stable along the walkway. Specifically, it was around 50 mg/m^3 on average upwind of the chock movement and there was an increase of dust concentration at about 15 m away from the tail gate as a result of ventilation backflow from the goaf, bringing a certain amount of dust back to the face. The dust concentration remained gently stable at around 50 mg/m^3 at more than 40 m away from the tail gate upwind of the chock movement.

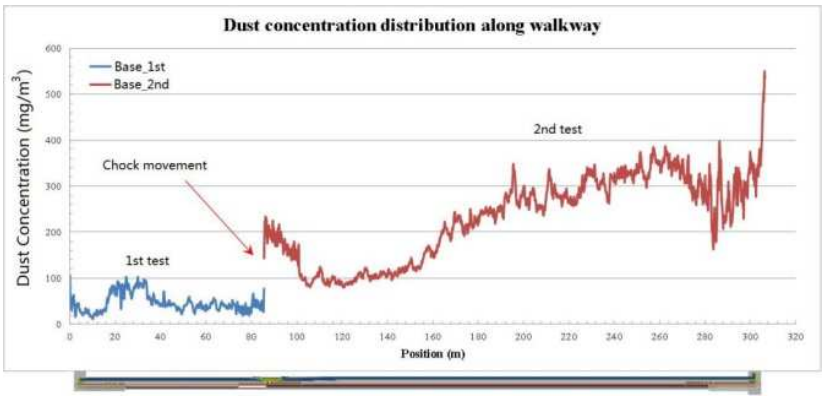

Figure 8 Dust concentration distribution along the walkway.

A significant increase in the dust concentration was also observed (up to 200 mg/m^3) immediately downwind of the chock movement, after which it dropped gradually to around 100 mg/m^3 at 100 m away from the tail gate. Due to the occurrence of coal spalling at the face's middle, there was a gradual increase of dust concentration starting at 150 m away from the tail gate. At the intersection of the face and the main gate, the dust concentration varied between 200 and 400 mg/m^3.

4 Development of a Dust Mitigation System

4.1 Design

Based on the understandings obtained from Section 4, effective dust mitigation strategies are required to reduce the dust level in the vicinity of the shearer and the main gate, and therefore, in this section a new dust mitigation system is proposed aimed at reducing dust levels around the shearer and at the main gate.

Figure 9 shows the design of the new dust mitigation system, which involves a shearer scrubber installed on the tail-gate (intake ventilation) side of the shearer (Figure 9(a)), a BSL scrubber on top of the crusher at the main gate (Figure 9(b)), and a new curtain connecting the existing curtain to the BSL scrubber inlet, as indicated in Figure 9(c).

It is worth noting that the capacity of the shearer scrubber used in the model is 4.5 m^3/s and the BSL scrubber capacity is 15 m^3/s, considering the extremely high dust concentration at the main gate.

4.2 Air Flow Patterns

Figure 10 depicts the velocity contour and vector distribution at 3 m above floor level in the vicinity of the shearer. It can be observed that the operation of the scrubber has a significant impact on the local airflow patterns. With the scrubber inlet facing directly toward the intake ventilation, the majority of dust laden air can be sucked into the scrubber system and with the assistance of scrubber sprays, the influencing area of the scrubber can be enlarged by which more air is directed to the flow towards the scrubber inlet, as shown in the figures. It is also noticed that a low pressure zone can be generated downstream, where the air flows towards the face as well as the dust particles in the air, and this will help to some extent in reducing the dust level in the walkway.

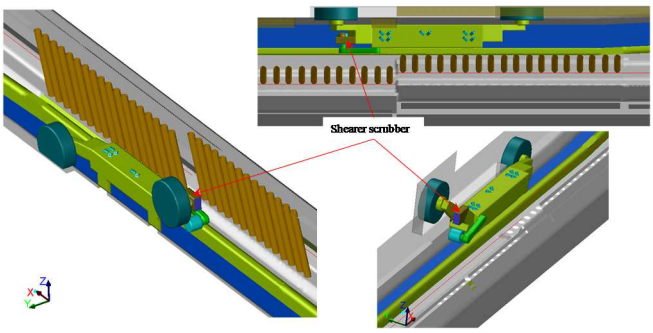

(a) Shearer scrubber

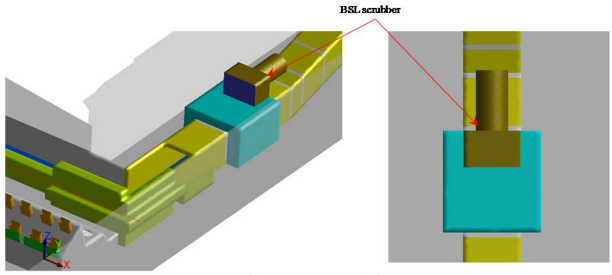

(b) BSL scrubber

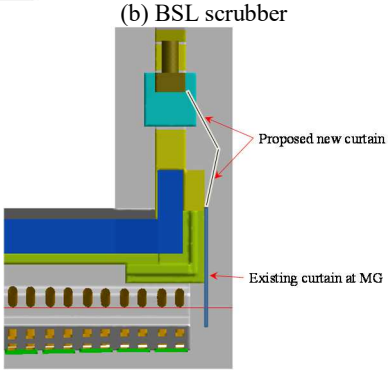

(c) Curtain at main gate

Figure 9 Design of a new dust mitigation system.

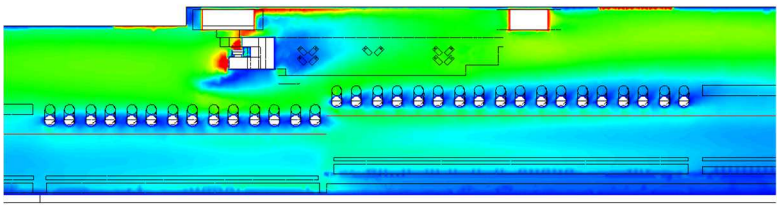

Figure 10 Velocity contour at 3 m above floor level (across from the scrubber inlet).

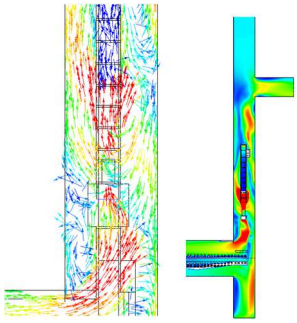

Figure 11 Velocity distribution at 2.5 m above floor level (in the vicinity of the BSL scrubber).

Figure 11 illustrates the velocity distribution at 2.5 m above floor level in the vicinity of the BSL scrubber. It can be seen that the velocity is not evenly distributed in the main gate and the majority of the dust laden air from the face will be directed to the scrubber inlet with the assistance of the new curtain, making it possible to capture the majority of dust particles from the face. It is also noticed that flow circulation occurs due to the high velocity at the scrubber outlet; however, this will not affect the quality of the ventilation at the main gate as air from the scrubber outlet is generally clean.

4.3 Respirable Dust Flow and Distribution Patterns

The dispersion of dust particles from the face spalling and leading drum cutting is illustrated in Figure 11 to evaluate the performance of the shearer scrubber. The effectiveness of the scrubber can be clearly seen from Figure 12. It is observed that when the scrubber is operating, the majority of the dust particles can be captured by the scrubber system. The amount of particles dispersing into the walkway and further downstream of the shearer is thus minimized, contributing to the reduction of the dust concentration along the face. It is worth noting that the shearer scrubber will be very effective in capturing dust particles from upwind (e.g. intake ventilation, spalling ahead of it and tail gate drum cutting).

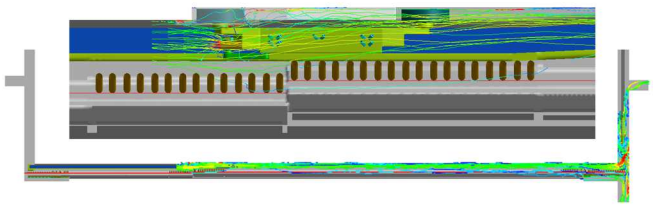

Figure 12 Dispersion characteristics of dust particles from the face spalling and leading drum cutting.

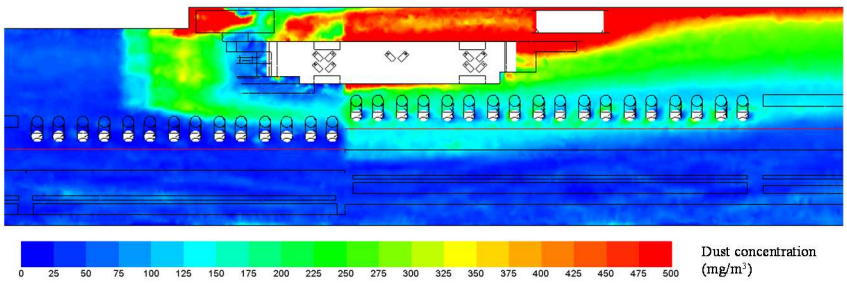

Figure 13 Dust concentration distribution at 2.5 m above floor level.

The dust concentration distribution in the vicinity of the shearer and the BSL is illustrated in Figure 13. It can be seen from Figure 13 that the dust concentration around the shearer scrubber and downstream from it can be reduced greatly from more than 500 mg/m^3 to around 200 mg/m^3. The dust concentration in the walkway is also reduced slightly.

Figure 14 shows the impact of the new scrubber system on dust mitigation along the walkway. It can be seen from Figure 14 that the dust concentration can be reduced by 50 to 100 mg/m^3 in the walkway downwind of the chock movement, while its effect is marginal in other areas along the walkway, i.e. upwind of the chock movement and at the intersection of the face and the main gate.

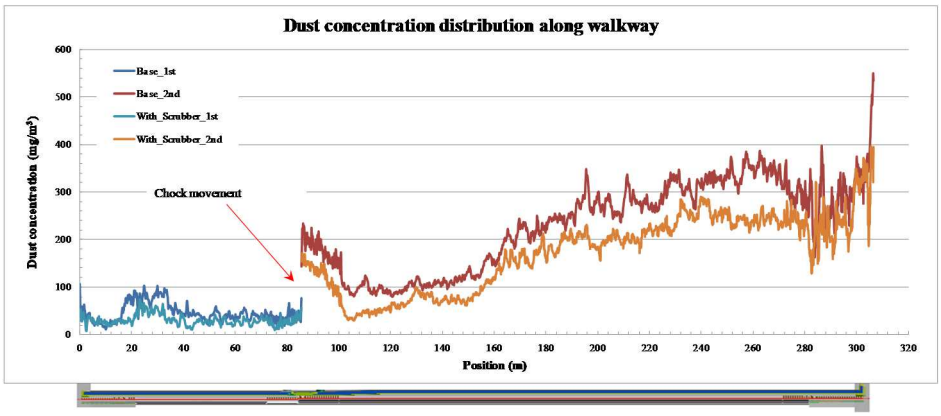

Figure 14 Dust concentration distribution along the walkway.

5 Conclusions

To address the issue of high dust concentration at the longwall faces of the Shihe colliery, field testing and CFD modeling were conducted to understand the exact sources of dust generation and its dynamic movement at the #5301 high longwall face of the colliery. The investigation included dust testing, a ventilation survey, and CFD modeling. The results of this investigation were then used to develop an effective dust mitigation system for the face. When the control system was trialed on site, the dust control effect turned out to be excellent.

The average dust load at both the last open cut through and the intake roadway was 0.0004 mg/t, and the dust loads at shields #173, #85 and #4 were 0.0005 mg/t, 0.0033 mg/t and 0.0051 mg/t respectively.

A CFD longwall model was developed based on information collected during field tests and the modeling results indicate that the air flow velocity is not evenly distributed over the cross sections along the face, with the highest velocity occurring above the spill plate and the AFC, and velocity dropping gradually from the face to the goaf side.

The new dust mitigation design involves the installation of a shearer scrubber of 4.5 m^3/s capacity on the tail gate side of the shearer, the installation of crescent sprays on the main gate side of shearer, the installation of flat venture sprays on the flipper of each chock, the installation of a BSL scrubber of 8 m^3/s capacity on top of the crusher at the main gate, the installation of a new curtain connecting the existing curtain to the BSL scrubber inlet, and the installation of sprays in the crusher, BSL and BSL discharge.

The modeled results with the new dust mitigation design indicate that the operation of the shearer scrubber will have a significant impact on the local air flow patterns, maximizing the influencing area of the scrubber and allowing more dust particles from upwind ventilation to be captured. Airflows towards the face immediately downstream of the shearer scrubber will help to some extent in reducing the dust level in the walkway and the majority of dust laden air will be directed towards the BSL scrubber inlet with the assistance of a new curtain at the main gate.

References

[1] National Institute of Occupational Safety and Health (NIOSH), *Best Practices for Dust Control in Coal Mining*, Pub. No. 2010-110, Pittsburgh, PA:NIOSH, USA, 2010.

[2] Petsonk, E.L., Rose, C. & Cohen, R., *Coal Mine Dust Lung Disease*, American Journal of Respiratory and Clinical Care Medicine, **187**(11), pp. 1178-1185, 2013.
[3] Zheng, Y.P., Feng, C.G., Jing, G.X., Qian, X.M., Li, X.J., Liu, Z.Y. & Huang, P., *A Statistical Analysis of Coal Mine Accidents Caused by Coal Dust Explosions in China*, Journal of Loss Prevention in the Process Industries, **22**(4), pp. 528-532, 2009.
[4] China National Health and Family Planning Commission (CNHFPC), *Bulletin for Occupational Disease Prevention and Control Work in 2009-2014*, Beijing, China (in Chinese), 2015.
[5] State Administration of Coal Mine Safety (SACMS), *Safety Regulations in Coal Mines 2008*, Beijing, China (in Chinese), 2008.
[6] New South Wales Government, *Notice-Airborne Dust Limits, Collection and Analysis*, Sydney, Australia, 2007.
[7] Colinet, J.F., Rider, J.P., Listak, J.M., Organiscak, J.A. & Wolfe, A.L., *Best Practices for Dust Control in Coal Mining*, United States Information Circular 9517, National Institute for Occupational Safety and Health (NIOSH), Pittsburgh, USA, 2010.
[8] Plush, B., Ren, T. & Aziz, N., *A Critical Evaluation of Dust Sampling Methodologies in Longwall Mining in Australia and the USA*, In: Aziz, N. (ed.) 12th Underground Coal Operators Conference, University of Wollongong, Wollongong, Australia, 2012.
[9] Aziz, N., Cram, K. & Hewitt, A., *Mine Dust and Dust Suppression*, In: Kininmonth, R.J. and Baafi, E.Y. (eds.), *Australian Coal Mining Practice,* Third ed.: Australasian Institute of Mining and Metallurgy, Melbourne, Australia, 2009.
[10] McPherson, M.J., *Subsurface Ventilation Engineering (2nd edition),* Published by Mine Ventilation Services Inc., Fresno, California, USA, 2009.
[11] Wang, H., Wang, D., Lu, X., Gao, Q., Ren, W. & Zhang, Y., *Experimental Investigation of the Performance of a New Design of Foaming Agent Adding Device Used for Dust Control in Underground Coal Mines,* Journal of Loss Prevention in the Process Industries, **25**(6), pp. 1075-1084, 2012.
[12] Wang, H., Wang, D., Tang, Y., Qin, B. & Xin, H., *Experimental Investigation of the Performance of a Novel Foam Generator for Dust Suppression In Underground Coal Mines*, Advanced Powder Technology, **25**(3), pp. 1053-1059, 2014.
[13] Goodman, G.V.R., *Using Water Sprays to Improve Performance of a Flooded-Bed Dust Scrubber,* Applied Occupational and Environmental Hygiene, **15**(7), pp. 550-560, 2000.

[14] Pollock, D. & Organiscak, J., *Airborne Dust Capture and Induced Airflow of Various Spray Nozzle Designs*, Aerosol Science and Technology, **41**(7), pp. 711-720, 2007.
[15] Lauder, B.E. & Spalding, D.B., *Mathematical Models of Turbulence*, Academic Press, 1972.
[16] Hargreaves, D.M. & Lowndes, I.S., *The Computational Modeling of the Ventilation Flows Within a Rapid Development Drivage*, *Tunnelling and Underground Space Technology*, **22**(2), pp. 150-160, 2007.
[17] Moloney, K.W. & Lowndes, I.S., *Comparison of Measured Underground Air Velocities and Air Flows Simulated by Computational Fluid Dynamics*, Trans. Inst. Min. Metall. Sect. A – Min. Technol., **108**, pp. A105-A114, 1999.
[18] Ren, T., Wang, Z. & Cooper, G., *CFD Modeling of Ventilation and Dust Flow Behavior Above an Underground Bin and the Design of an Innovative Dust Mitigation System*, Tunnelling and Underground Space Technology, **41**, pp. 241-254, 2014.
[19] Torano, J., Torno, S., Menendez, M. & Gent, M., *Auxiliary Ventilation in Mining Roadways Driven with Roadheaders: Validated CFD Modeling of Dust Behavior*, Tunnelling and Underground Space Technology, **26(1)**, pp. 201-210, 2011.
[20] ANSYS, *Fluent Theory Guide*, Release 13, ANSYS Inc, 2010.